applied sciences

MDPI

Article

Testing and Analysis of the Vibration Response Characteristics of Heavy-Haul Railway Tunnels and Surrounding Soil with Base Voids

Liping Gao, Jianjun Luo *, Tielin Chen, Dengke Wang and Guanqing Wang

Key Laboratory for Urban Underground Engineering of Ministry of Education, Beijing Jiaotong University, Beijing 100044, China

* Correspondence: jjluo@bjtu.edu.cn; Tel.: +86-136-1130-3609

Abstract: This paper discusses research on the dynamic response characteristics of a heavy-haul railway tunnel and the surrounding soil under the conditions of substrate health and a base void. The detection results of the base condition of 20 double-track tunnels for a heavy-haul railway show the main distribution law of base voids. Based on this, a 1:20 scale test model of a heavy-haul railway tunnel is established. The vibration load of the train is established by a vibration exciter arranged at the tunnel invert. The dynamic response and attenuation law of a heavy-haul railway tunnel lining structure and the surrounding soil are tested using acceleration sensors, strain gauges, and soil pressure boxes. The research results show that most of the diseases are concentrated below the heavy-haul line. The base void causes the peak acceleration of the nearby tunnel invert to increase by 55.6%. Tunnel annular construction joints reduce the conductivity of the vibration waves in the axial direction of the tunnel. The acceleration attenuation rate of the soil above the tunnel invert is significantly less than that under the invert. The base void reduces the acceleration of the nearby soil layer by 19.4% and increases the stress on the surface of the nearby tunnel invert by 21.3%, and the stress change amplitude increases by 0.55%. The tunnel structure in the area of the base void experiences fatigue damage. The base void causes the compaction and bearing capacity of the nearby soil to decrease and the softening speed of the tunnel basement soil layer to increase. Therefore, for the basement damage to heavy-haul railway tunnels, "early detection, early treatment" should be performed.

Keywords: tunnelling structure; heavy-haul railway; model test; train vibration load; dynamic response

check for updates

Citation: Gao, L.; Luo, J.; Chen, T.; Wang, D.; Wang, G. Testing and Analysis of the Vibration Response Characteristics of Heavy-Haul Railway Tunnels and Surrounding Soil with Base Voids. *Appl. Sci.* **2023**, *13*, 4090. https://doi.org/10.3390/app13074090

Academic Editor: Daniel Dias

Received: 9 March 2023
Revised: 19 March 2023
Accepted: 20 March 2023
Published: 23 March 2023

Copyright: © 2023 by the authors. Licensee MDPI, Basel, Switzerland. This article is an open access article distributed under the terms and conditions of the Creative Commons Attribution (CC BY) license (https://creativecommons.org/licenses/by/4.0/).

1. Introduction

With the rapid development of China's economy, the role of heavy-haul railway transportation in promoting national economic development has become increasingly more important [1]. Compared with traditional railways, heavy-haul railways have the characteristics of large shafts, high opening density, and greater vibration loads on the base of a tunnel. Therefore, the bottom structure of a tunnel is more prone to damage [2,3]. According to the research of relevant references, the main contradiction in the substrate quality of heavy-haul railway tunnels in operation in China lies in the contradiction between the increasing weight of the train axle and the resulting substrate damage. The main manifestations are that with the long-term repeated vibration of heavy-haul trains and groundwater seepage, the small defects in the tunnel substrate have evolved into structural and softening between surrounding rocks, and even damage such as emptying, arching, and filling layer cracking or staggered platforms, slurry, and mud.

Softening and the void between the tunnel invert and surrounding rock is a major form of basement damage. The first reason for this is that the early tunnels in China lacked forward-looking design, and insufficient attention was paid to the design of the tunnel drainage structure. Over time, the only drainage pipes become blocked by impurities,

and the groundwater that cannot be discharged smoothly forms a "scouring" effect on the surrounding rock. In addition to the poor construction quality of some tunnels, the gap between the basement structure and the surrounding rock creates "congenital defects". The second reason is that the repeated action of the groundwater and train load causes the enhancement of the surrounding rock liquefaction liquidity. The rock mass is constantly "emptied" with the action of seepage, and the created base voids increase. Once the tunnel base voids appear, it greatly weakens the stress performance of the structure, induces inverted arch cracking and damage, and even causes a large-scale fracture, staggered platform, or collapse of the structure at the bottom of the tunnel, which will worsen driving conditions and seriously affect transportation efficiency and driving safety. Base voids are still some of the important factors causing damage to the upper structure of a tunnel. Therefore, it is of great significance to study the vibration response of heavy-haul train railway tunnels with base voids.

For the dynamic response and fatigue damage life analysis of the substrate structure of heavy-haul railway tunnels, researchers studying this topic in China have conducted in-depth research. Zou Wenhao [4] combined on-site measured data and a numerical simulation, and the dynamic response law of the substrate structure of a tunnel with the action of a load of a 30 t axle heavy train was studied. It was proven that the numerical simulation results could be generally consistent with the actual measurement trend in the field. The dynamic stress response of the base structure on the side of the heavy load line of the tunnel structure was significantly greater than that on the side of the empty train line, and the stress performances of different forms of tunnel inverts were analyzed. Xue Jilian [5] analyzed the cause of the tunnel bottom structure, and the dynamic response of the tunnel bottom structure reinforced by polyurethane with the action of 30 t axle heavy trains was studied using finite element software. Yin Chengfei et al. [6] combined the composite lining tunnel of the Shuohuang Railway, studied the dynamic stress changes in different positions of the filling layer and inverts of the heavy-haul railway tunnel. Ding Zude [7] applied a concrete plastic damage model to analyze the stress level and damage value of a tunnel invert with different base voids for a heavy-haul railway tunnel. When the lateral base void reached 120 cm, the damage value of the bottom structure reached 1.0. Deng Bin [8] established a numerical analysis model and analyzed the dynamic response characteristics of the laying structure of a heavy-haul railway tunnel with different laying thicknesses with the action of a 30 t axis heavy train load. Xu Xinli [9] established a three-dimensional dynamic analysis model for a tunnel, and the stress state and fatigue life of the substrate structure of the full-frame and half-frame heavy-haul train tunnel were studied. Liu Ning [10] applied the Miner linear fatigue accumulation damage criterion and calculated the service life law of the substrate structure of heavy-haul tunnels for different substrate softening and base void conditions. It was proven that the degree of base void significantly affected the fatigue life of the tunnel structure. Lihui Xu et al. [11] proposed a novel coupled periodic tunnel–soil analytical model for predicting ground-borne vibrations caused by vibration sources in tunnels. Xuming Li et al. [12] proposed a hybrid approach that combined the Bayesian Neural Network and the impedance model to predict vibrations inside a building by considering the coupling loss of soil and building structure. Zou, C. et al. [13] developed an efficient computational model that characterizes the dominant mode of vibration transmission through each structural element including those in transfer structures in building designs where ground and building columns are not aligned.

In summary, a certain amount of scientific research has been carried out on the vibration response and damage development law of the base structure of a heavy-haul railway. However, numerical simulation analysis is mostly used in the study of heavy-haul railway tunnel damage, and the accuracy of the calculation results needs to be tested. There are very few existing tests on the dynamic response of a heavy-haul railway tunnel structure and the surrounding soil layers. Based on the statistical results of a heavy-haul railway tunnel, a 1:20 scale tunnel model test is established in this research. Single-point excitation

vibration is used to simulate the overloaded train load. The dynamic response characteristics of the tunnel structure and the surrounding soil layer are studied under the conditions of substrate health and a base void using an acceleration sensor, strain gauge, and soil pressure box.

2. Detection of Tunnel Base Voids

At the time of this research, all of the 20 single-hole and double-line tunnels with the detected prominent base damage problems are from a special heavy-haul railway for coal transport that has been in service for more than 30 years. The tunnels are mainly of short–medium length. The cumulative length of the measured tunnel is 41,102 m. The tunnel length accounts for the largest proportion in the grade V surrounding rock environment, approximately 48.0%.

Geological radar is used to detect the voids and loose areas of a tunnel basement, and this radar mainly detects the scope, position, and scale. A typical base void radar effect diagram is shown in Figure 1. The statistical plots of the tunnel base voids are shown in Figures 2 and 3.

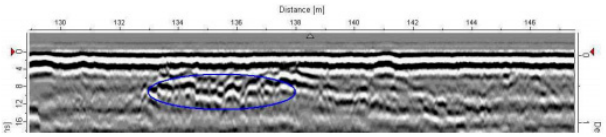


Figure 1. Typical radar map of base void.

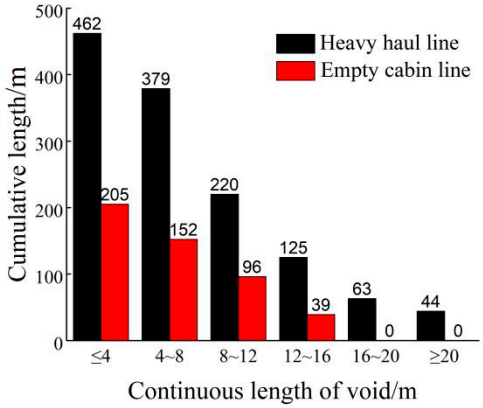


Figure 2. Cumulative length of tunnel with different base void lengths.

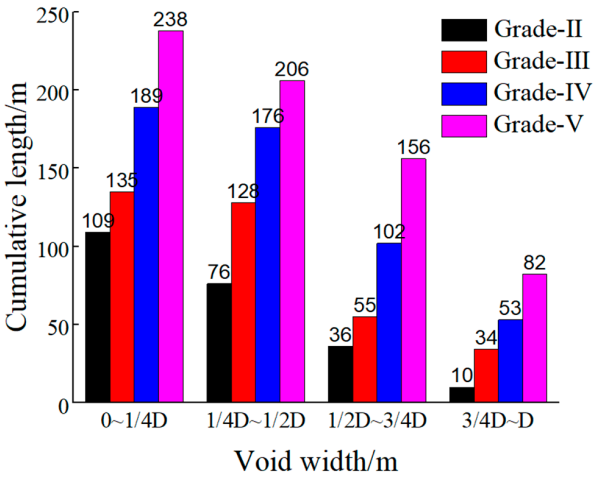


Figure 3. Cumulative length of tunnel with different base void widths.

From Figure 2, the average longitudinal length of the base voids below the tunnel's heavy-haul line is approximately 2.63 times that below the empty cabin line. The continuous base void length below the heavy-haul line is approximately 65.1% within the range of 0–8 m, and the ultra-long distance voids above 12 m also account for a considerable proportion.

Figure 3 shows the cumulative length statistical diagram of different widths corresponding to different surrounding rock levels. D is the effective width of the tunnel invert, that is, the widest transverse distance of the invert. From the general trend, the transverse void width of the base is mainly concentrated in the range of 0–1/2 D. The worse the tunnel damage interval is with the surrounding rock mass, the larger the base void width is. In grade IV surrounding rock, the base void widths of 1/2 D–3/4 D and 3/4 D–D account for 21.9% and 11.4%, respectively, while in grade V surrounding rock, the base void widths of 1/2 D–3/4 D and 3/4 D–D account for 22.9% and 12.1%, respectively.

In summary, the base voids of heavy-haul railway tunnels mostly occur in heavy-haul lines. The base void length is mostly concentrated in the range of 0–8 m, and the width is mostly concentrated in the range of 0–1/2 D. From grade II to grade V surrounding rocks, the cumulative value of the average base voids width increases by approximately 31.1%, 47.7%, and 52.3%.

3. Model Test Overview

3.1. Model-Trial Similarity Ratio

Considering the dynamic response of train loads to tunnels and foundation soil, the main cause for tunnel lining and surrounding formations under vibration loads is elastic deformation [14]. In similar studies, most of the assumptions are elastic tests. Although the base voids may cause a certain plastic deformation for a structure, compared with the actual running time of decades, the plastic deformation formed in the short term of the test is very small. Therefore, the test adopts the law of elastic similarity. In this experiment, this law mainly involves determining similar materials for surrounding rock and tunnel lining. According to the tunnel prototype, the basic similarity ratios of the foundation of the model are as follows: geometric similarity ratio $\alpha_L = 20$, density similarity ratio $\alpha_\rho = 1$, and elastic modulus similarity ratio $\alpha_E = 20$. The similarity ratio of other physical quantities can be obtained according to the similarity theory. The specific similarity relationship is shown in Table 1.

Table 1. Similarity ratio of each physical quantity.

Physical Quantity	Similarity Ratio Expression	Similarity Ratio (Model: Prototype)
Geometry	α_L	1:20
Density	α_ρ	1:1
Elastic modulus	α_E	1:20
Acceleration	$\alpha_E\alpha_l{}^{-1}\alpha_\rho{}^{-1}$	1:1
Time	$\alpha_l\alpha_\rho{}^{1/2}\alpha_E{}^{-1/2}$	1: 4.47
Frequency	$a_l{}^{-1}\alpha_\rho{}^{-1/2}\alpha_E{}^{1/2}$	4.47:1
Physical strength	$\alpha_\rho\alpha_l{}^3$	1: 8000
Stress/pressure	α_l	1:20

3.2. Preparation of the Model

3.2.1. Similarity Materials of Tunnel and Soil

The deformation of the tunnel lining and surrounding rocks is mainly within the range of elastic deformation. To meet the material requirements for the shrinkage model test, the density, Poisson ratio, and elastic modulus are the main control parameters.

Because the fracture performance of gypsum is similar to that of concrete [15], it is a more common method in the proportional model experiment [16]. The standard cylinder model is equipped with different proportions of gypsum, diatomite, and water mass. After processing, the mold density is calculated by weighing, and the elastic modulus

and compressive strength of gypsum of different proportion materials are tested with a universal experimental machine.

During the test, it is found that the performance of gypsum mixed with diatomite does not change significantly. Due to the rapid initial coagulation speed of high-strength gypsum, the short mixing time of the material will cause an uneven stirring of diatomite and affect the performance of the material. If the mixing time is too long, the slurry will become thicker, resulting in defects of mold stratification and unequal density. In summary, only the mixture of high-strength gypsum and water is used in this experiment. Considering the simulated C30 concrete, the final configuration scheme of high-strength gypsum and a water mass ratio of 1:0.9 is adopted. The physical and mechanical parameters of the tunnel structure are shown in Table 2.

Table 2. Physical and mechanical parameters of tunnel materials.

Type	Density (kg·m^{-3})	Elastic Modulus (MPa)	Poisson Ratio
Prototype	2300	31.5	0.3
model	2300	1.58	0.3

The parameters of the surrounding rock for the prototype are sourced from the survey report related to the measured tunnel. To bring the configuration material as close to the surrounding rock of the soil as much as possible, after multiple configuration experiments, it is finally determined that quartz sand and river sand are used as aggregates, and fly ash and Vaseline are added as harmonic binders. The configuration ratio (mass ratio) is finally determined to be quartz sand:river sand:fly ash:Vaseline = 15:13.5:6:1. The configuration materials and parameters of the surrounding rock for the prototype are shown in Table 3.

Table 3. Physical and mechanical parameters of surrounding rock materials.

	Density	Elastic Modulus	Poisson Ratio	Internal Friction Angle	Cohesion
	(kN·m^{-3})	E (MPa)	μ	φ (°)	c (kPa)
Prototype materials	1900	400	0.31	28	130
Model materials	1900	20	0.31	29	6.5

3.2.2. Simulation of Circumferential Construction Joints

The realistic molded lining circumferential construction joints are designed according to an 8–12 m range for construction, and the entire joint is set. Because the existence of construction conditions may affect the propagation of an axial vibration wave in the tunnel, the construction joint is designed according to the actual 10 m. The corresponding model is 50 cm high per pouring and paused for 3 min so that the poured gypsum can continue to be poured after the initial condensation. The tunnel model is 150 cm long with a total of two "construction joints". The section of the prototype tunnel is sourced from a heavy-load, single-hole bidirectional tunnel in Inner Mongolia. The section is a horseshoe-shaped, plain concrete structure. The section dimensions are shown in Figure 4. The process of tunnel model fabrication is shown in Figure 5.

3.3. Installation of Test Devices and Measuring Points

This experiment provides a simulation system for the vibration response of the basement structure of a heavy-haul railway tunnel. The test device is mainly composed of four parts: (1) The model box is used to simulate tunnels and surrounding rock. The length, width, and height dimensions of the box are 3.0 × 1.5 × 2 m. (2) Load generation devices are used to simulate the train load, which include a single-point exciter and its supporting power amplifier. (3) A data acquisition and storage system collects and stores

sensor information in real time. Acceleration sensors, strain gauges, soil pressure boxes, and a force sensor are used in this test. (4) For the control system, the vibration signal is managed by a computer to control the output force and frequency of the exciter.

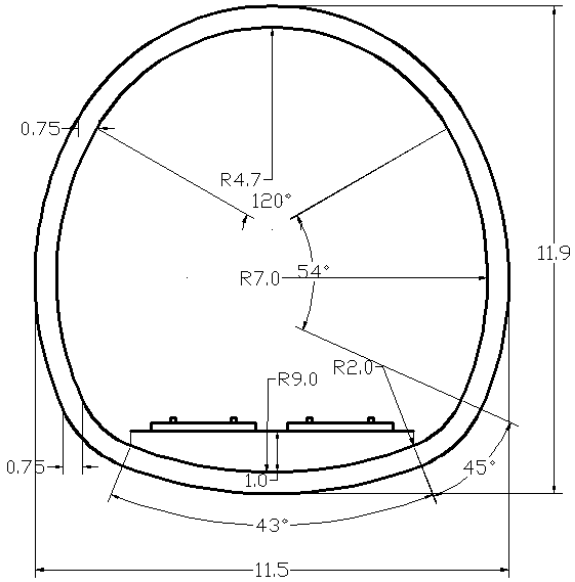


Figure 4. Dimensions of tunnel section (m).



(**a**) (**b**) (**c**) (**d**)

Figure 5. The production process of the lining model: (**a**) positioning and assembling; (**b**) brushing the oil; (**c**) slurry stirring; (**d**) perfusion model.

To facilitate the observation of the state of the tunnel model during the experiment, a 1.5 m × 1.5 m plexiglass panel observation window is set on one side of the model box. The observation window has an opening according to the inner diameter of the tunnel model, and the other positions are steel plates. The pressure of the material used in the bench is greater than 0.3 MPa, and the structural deformation within this force range does not exceed 0.3 mm, which meets the required conditions for the test. The longitudinal length of the tunnel model is 1.5 m, the thickness of the overburdened soil layer is 0.5 m (corresponding to the buried depth of the prototype of 10 m), and the thickness of the lower soil is 80 cm (corresponding to the prototype thickness of 16 m). For the vibration tests, it is necessary to consider the impact of the reflection of the boundary wave of the model box on the experimental results. Duxseal is a vibration-absorbing material widely used around the world. It can absorb both shear and compression waves. The absorption effect is directly related to the thickness of the material laying. Based on the research experience of predecessors, the Duxseal material with a thickness of 3 cm is bonded to the side of the box [14,17]. The model test bench is shown in Figure 6.

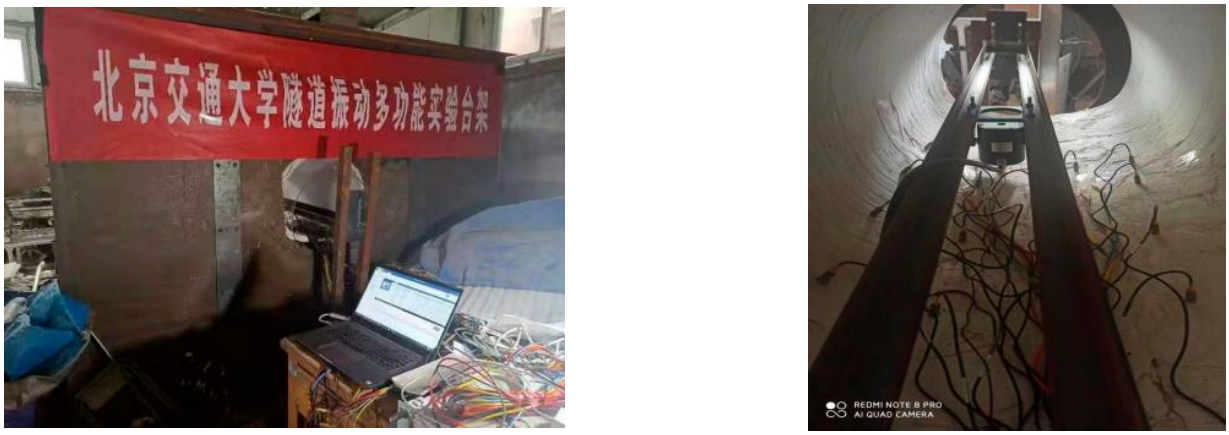


Figure 6. Model test bench.

The model test uses an exciter to apply a vibration load. According to the law of driving a heavy-haul on one side, the exciter is arranged 10 cm to the left of the middle line of the tunnel model. The upper part of the exciter is fixed in place on the reaction frame. The contact between the exciter and the tunnel model can be controlled by finely adjusting the height of the anti-force frame. A force sensor is installed at the lower end of the excitation device to collect the vibration load applied by the excitation device at the bottom of the tunnel model.

To obtain the dynamic response of heavy-haul railway tunnels and the surrounding soil layers with the vibration load of trains, sensors are installed in the tunnel and the surrounding soil layers. The layout of the acceleration sensor in the tunnel is shown in Figure 7, and the acceleration sensor in the soil layer is shown in Figure 8. The strain sheets are arranged symmetrically on both sides of the tunnel invert, as shown in Figure 9. The soil pressure cell is arranged in the soil layer, as shown in Figure 10.

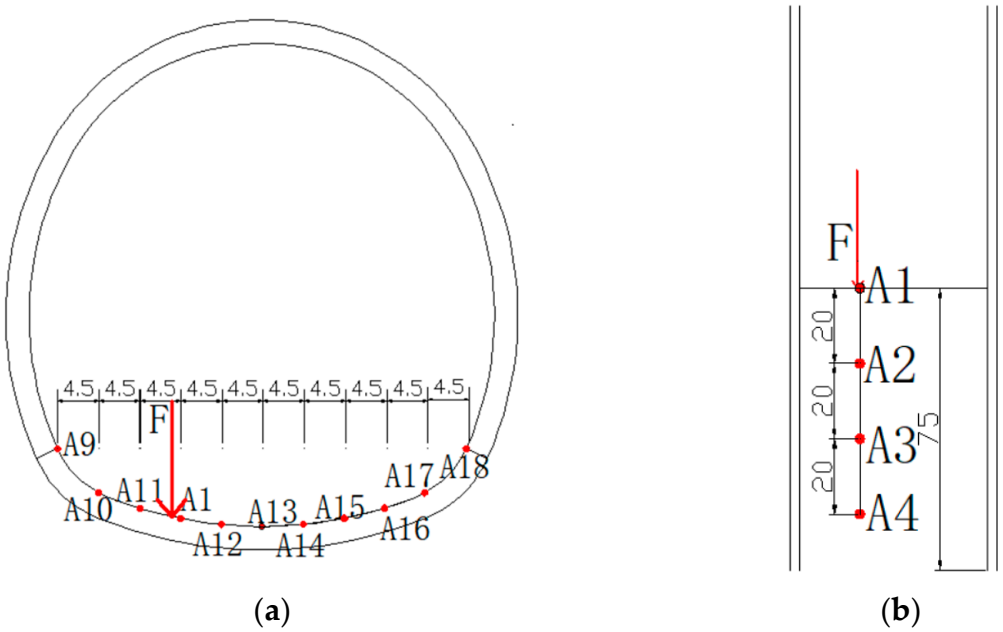


Figure 7. The layout of the acceleration sensor in the tunnel (cm): (**a**) annular layout; (**b**) axial layout on the tunnel invert.

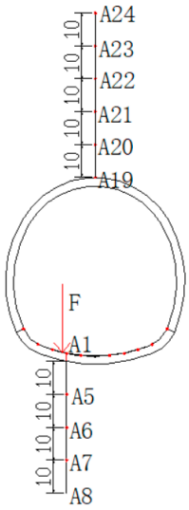


Figure 8. The layout of the acceleration sensor in the soil layer (cm).

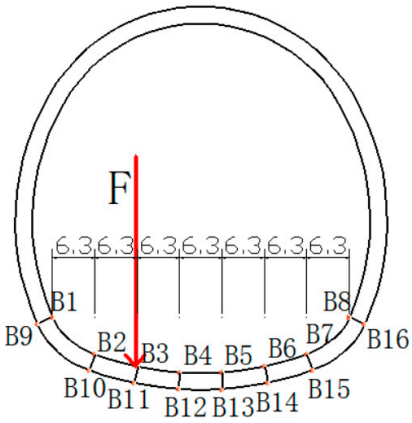


Figure 9. The layout of strain sheet (cm).

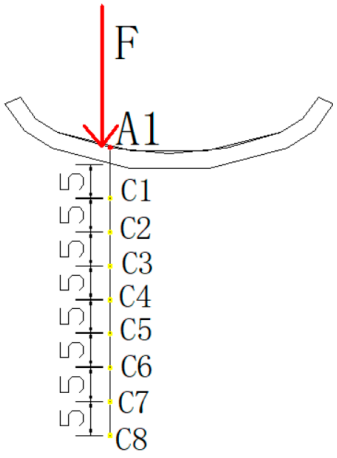


Figure 10. The layout of soil pressure cell (cm).

3.4. Testing Program

3.4.1. Base Conditions

According to the statistical results of the detection of basement damage to heavy-haul railway tunnels, the operability of the test is also considered. The tunnel substrate conditions are determined as the base without a void and the base with a void below the

vibrating load. The void depth of the soil under the model tunnel invert is 1 cm, and the axial length of void is 20 cm, as shown in Figure 11.

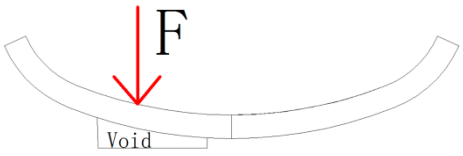


Figure 11. Schematic of the base void.

3.4.2. Input of Load Capacity

To simulate the dynamic response characteristics of the tunnel structure and surrounding soil layer when heavy-haul trains pass through the tunnel, the vibration load of the 30 t axis heavy train is used in the test. The vibration load of heavy-haul trains is simulated by the internationally accepted excitation load function formula, which includes both the static load of the train and the dynamic load considering the uneven track, rail wear, and mechanical transfer state of the rail. The function formula is

$$F(t) = k_1 k_2 [P_0 + P_1 \sin \omega_1 t + P_2 \sin \omega_2 t + P_3 \sin \omega_3 t] \quad (1)$$

In the expression,

$$P_i = m a_i \omega_i^2,\ i = 1,2,3$$
$$\omega_i = 2\pi v / L_i$$

k_1 is the wheel–rail force superposition coefficient. k_2 is the steel rail dispersion transfer coefficient. k_1 and k_2 can be calculated according to conditions such as the vehicle type and track structure. Generally, the k_1 value range is 1.2–1.7, and the k_2 range is 0.6–0.9. In this research, k_1 is 1.54, k_2 is 0.7 and P_0 is the wheel self-weight static load. P_0 of the 30 t axis heavy-haul train is 150 kN. P_1, P_2, and P_3 are the dynamic loads related to track irregularities, the dynamic additional load, and the waveform wear, respectively. m is the unsprung mass of the train, obtained as 750 kg. L_i and a_i are the managed value and typical vector height, respectively. In reference [18], L_1 = 10 m, a_1 = 3.5 mm, L_2 = 2 m, a_2 = 0.4 mm, L_3 = 0.5 m, and a_3 = 0.08 mm. v is the train running speed, and v = 80 km/h = 22.2 m/s is used for a convenient calculation. According to Formula 1, the artificial excitation load time curve of the 30 t axis heavy train at a running speed of 80 km/h is shown in Figure 12. However, the vibrator cannot output a complex changing force, so the maximum force is used as shown in Figure 12. At the speed of v = 80 km/h, the contact frequency between the train and the track is approximately 8 Hz, and according to the correlation coefficient of Table 1, the model test frequency is approximately 36 Hz. The train vibration load of the model test input vibrator is shown in Figure 13.

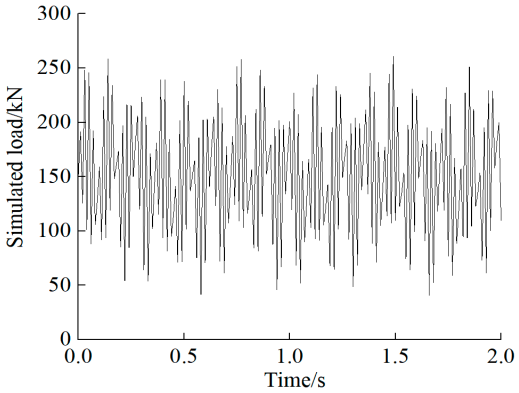


Figure 12. Time history curve of simulated train load.

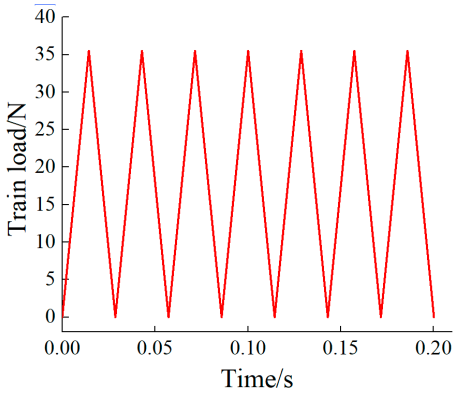


Figure 13. Simulated train load.

4. Analysis of the Dynamic Response Characteristics of Tunnel Lining

The accuracy of vibration test results is easily disturbed by the external environment. To minimize environmental interference, the experiment is performed at night. When analyzing the data, abnormal data are removed.

4.1. Acceleration Response Analysis of Tunnel Lining with Vibration Load

Figure 14 shows the acceleration time curve of the axial measurement points in the tunnel structure. Table 4 displays the peak values of acceleration of the axial measurement points of the tunnel. From Figure 14, it can be seen that there are significant differences in the peak value of the acceleration at different measurement points. The farther away the measuring point is from the vibration source, the smaller the acceleration response is. The peak acceleration of test point A1 is 3.11 m/s^2, a 55.6% increase over that when the base does not have a void. This indicates that the base voids significantly amplify the vibration response of the structure in the void region. Points A2–A4 are outside the base void range, and the peak acceleration growth rate is significantly smaller than point A1. The farther away from the vibration source the location is, the lower the acceleration peak growth rate is.

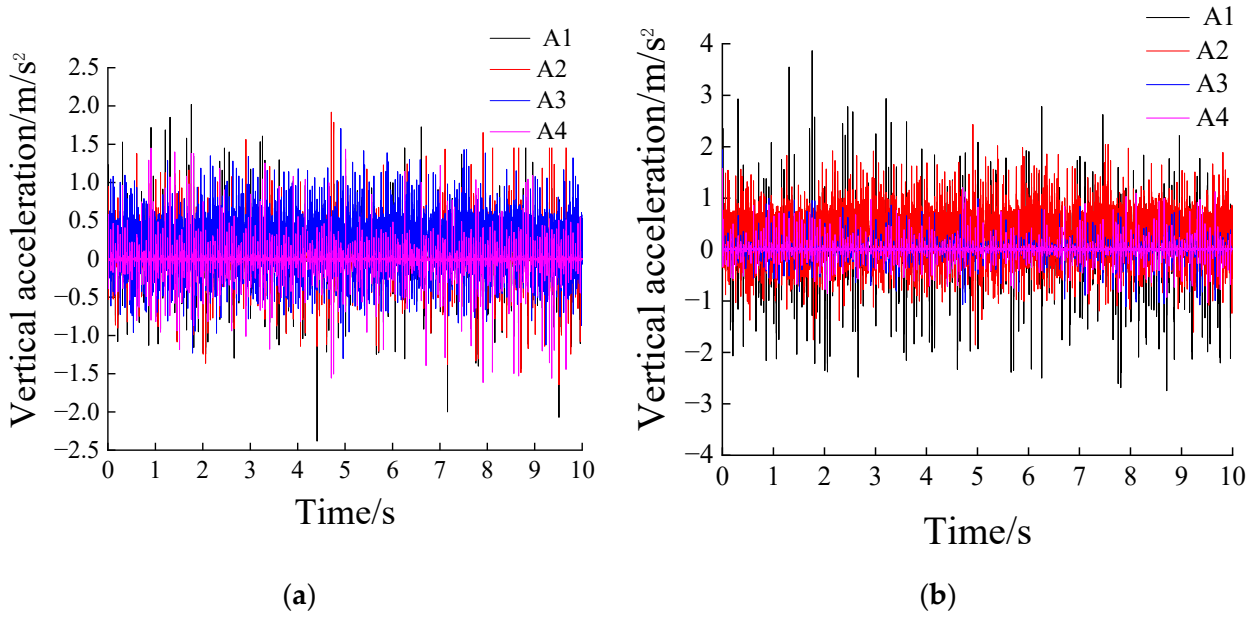


Figure 14. Acceleration time course curve of the tunnel axial measuring points: (**a**) no base void; (**b**) with base void.

Table 4. Statistics of peak acceleration of tunnel axial measuring point (m/s^2).

Type	No Base Void	With Base Void	Growth Rate (%)
A1	2.01	3.11	55.6
A2	1.73	2.11	21.9
A3	1.55	1.76	13.5
A4	1.34	1.58	8.9

Figure 15 shows the peak acceleration distribution of each measuring point of the tunnel invert. The blue line is the peak acceleration of each measuring point when the base does not have a void, and the red line is the peak acceleration of each measuring point when the base has a void. Because point A1 is closest to the vibration source, the peak value of the acceleration is the largest. The distance between the other points and the vibration source increases, and the acceleration gradually decreases. When there is a void in the tunnel base, the peak acceleration of each measuring point increases. A1, A11, and A12 are within the range of the base void, and the acceleration growth is the most obvious, increasing by 55.6%, 53.7%, and 54.5%, respectively. The farther away the location is from the base void area, the smaller the peak acceleration increase in the measurement points is. The furthest test point A18 shows an increase of only approximately 9.4% in peak acceleration over that when the base does not have a void.

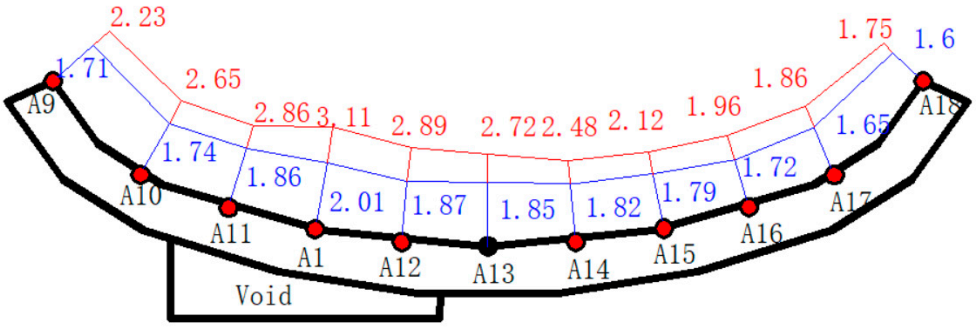


Figure 15. Peak value of the acceleration of each measuring point of the tunnel invert (m/s^2).

The decay rates of the peak acceleration of the tunnel invert measuring points are slightly slower than that of the axial measuring points in the tunnel. The main reason for this may be that the circumferential construction joints in the tunnel reduces the conduction efficiency of the vibration wave in the structure.

4.2. Analysis of Stress Change of Tunnel Invert with Vibration Load

Figure 16 shows the stress-time curve of the typical measuring points B3 and B11. It can be seen from the figure that the inner surface of the tunnel invert mainly has compressive stress, while the outer surface has tensile stress. The stress of the measuring point is constantly changing with the excitation load. When the base does not have a void, the amplitude of the compressive stress at point B3 is approximately 3.60 kPa, and that of point B11 is approximately 3.86 kPa. When the base has a void, the change amplitude of the compressive stress of point B3 is approximately 3.80 kPa, and that of point B11 is approximately 4.08 kPa. As is well known, the fatigue life of concrete is determined by the average stress and stress amplitude. The larger the two values become, the smaller the fatigue life of the structure then becomes. Therefore, the tunnel base voids will accelerate the structural fatigue damage.

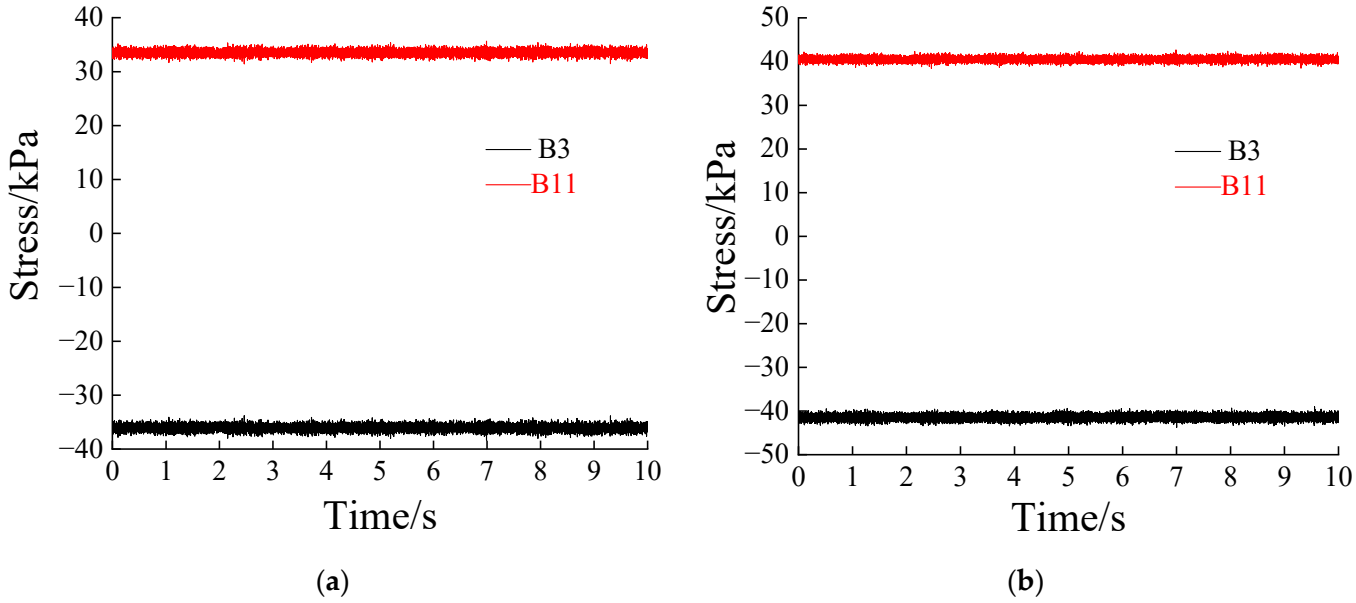


Figure 16. Stress-time curve of typical tunnel measurement points: (**a**) no base void; (**b**) with base void.

Table 5 lists the statistics of the peak stress at each measuring point of the tunnel invert. When the tunnel base has a void, the stress value of each measuring point of the tunnel invert increases. B2, B3, B4, B10, B11, and B12 are in the base void area, and the peak stress increase in the inverted arch is the most obvious. At this time, the stresses at points B3 and B11 are −41.8 kPa and 42.6 kPa, respectively, which are increases of 21.5% and 21.4%, respectively, from the stresses when the base does not have a void. The increase in the peak stress decreases significantly at the measuring points outside the base void range. The no-base-void measuring points B5 and B12 are the closest sites to the base void. Their peak stresses increase by only 5.4% and 5.7%. In contrast, for points B8 and B16, furthest from the void area, the peak stress barely increases.

Table 5. Peak stress at each measuring point of the tunnel invert (kPa).

Measuring Point	**B1**	**B2**	**B3**	**B4**	**B5**	**B6**	**B7**	**B8**
No base void	−26.5	−30.8	−34.4	−31.1	−27.6	−21.9	−20.1	−18.1
With base void	−29.0	−37.4	−41.8	−38.2	−29.1	−22.2	−20.6	−18.3
Measuring Point	**B1**	**B2**	**B3**	**B4**	**B5**	**B6**	**B7**	**B8**
No base void	25.9	31.9	35.1	31.5	28.2	22.3	20.4	18.5
With base void	29.2	38.3	42.6	38.8	29.8	22.5	20.9	18.6

The tensile strength design value of C30 concrete is f_t = 1.43 MPa [19], and the $\sigma_{max} > 1/2f_t$ structure suffers fatigue damage with the action of the cyclic load. According to Table 1, the stress similarity ratio is 1:20, and the diagram of the peak stress and allowable stress at the bottom of the tunnel invert is obtained (Figure 17). When the tunnel base does not have a void, the maximum tensile stress values of each measuring point at the bottom of the tunnel invert are all less than 715 kPa, and the tunnel structure does not produce fatigue damage with the action of the train load. When the tunnel base has a void, the tensile stress values of measuring points B10, B11, and B12 are greater than the allowable stress value, and the tunnel invert suffers fatigue damage with the long-term action of the train load.

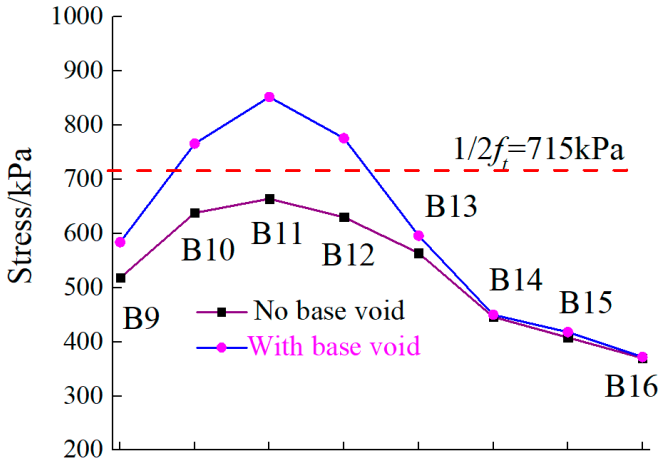


Figure 17. Relationship between peak stress and allowable stress at the measuring points of the invert.

5. Analysis of the Dynamic Response Characteristics of the Soil

5.1. Analysis of Acceleration of Soil with Vibration Load

Figure 18 shows the acceleration time curve of the soil layer below the tunnel invert. Table 6 displays the statistics of the peak acceleration of the soil layer below the tunnel invert. Similar to the tunnel structure, the acceleration of the soil points decreases as the distance from the vibration source increases. This is mainly because the existence of material damping causes the vibration wave in the propagation process. When the tunnel base has a void, the acceleration value of each measuring point in the soil layer decreases. This is mainly because the existence of the base void reduces the density of the vibration wave propagation medium and weakens the conduction efficiency of the vibration.

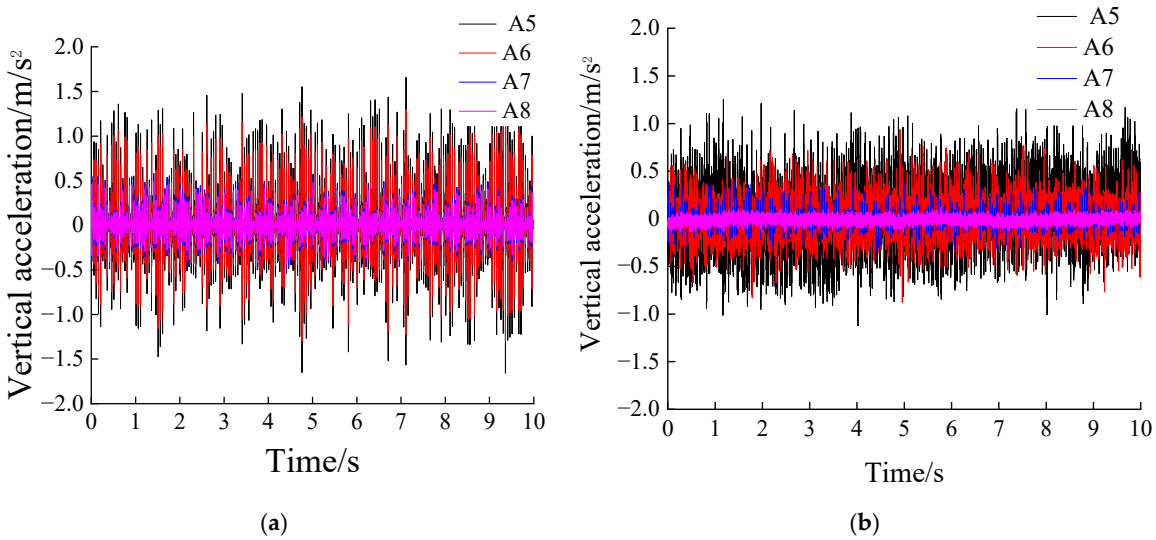


Figure 18. Acceleration time curve of soil measuring points below tunnel invert: (**a**) no base void; (**b**) with base void.

Table 6. Peak acceleration of soil layer measuring points (m/s^2).

Type	No Base Void	With Base Void	Growth Rate (%)
A5	1.55	1.25	19.4
A6	1.24	1.06	14.5
A7	0.86	0.79	8.1
A8	0.64	0.62	3.1

Figure 19 shows the peak acceleration of the soil layer points above the tunnel vault. The peak acceleration of each measuring point is significantly smaller than the peak acceleration of the soil layer below the tunnel invert. As the distance from the center of the source increases, the acceleration of different measuring points in the soil layer gradually decreases. The peak acceleration at point A20 is significantly smaller than that at point A19. The possible reason for this is that the measuring point A19 is close to the tunnel structure, and the vibration propagation efficiency of the tunnel is better than that of the soil layer. The peak acceleration of A20 is 0.21 m/s^2, and the peak acceleration of A23 is 0.11 m/s^2. Comparing the peak acceleration of measuring point A5 and measuring point A8, the decay rate of the acceleration of the soil layer above the vault is significantly reduced.

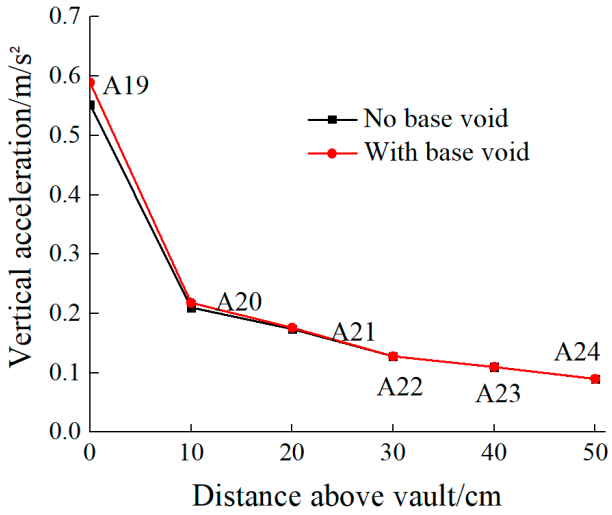


Figure 19. Peak acceleration of soil measurement points above the tunnel vault.

When the base has a void, the peak acceleration of measuring point A19 is 0.589 m/s^2, with an increase of 0.037 m/s^2 and a growth rate of approximately 6.7%. The A20 acceleration also increases slightly. However, the peak accelerations of measuring points A21–A24 are almost unchanged.

5.2. Analysis of Soil Pressure with Vibration Load

Figure 20 shows the peak vertical pressure of the soil layer below the tunnel invert. When the depth of the soil layer increases, the vertical pressure of each measuring point gradually increases. When the tunnel base has a void, the pressure of each measuring point is reduced to varying degrees. Measuring point C1 is the closest to the void area, and the vertical pressure is 6.46 kPa. Compared with the vertical pressure of 11.24 kPa when the base does not have a void, there is a decrease of 42.5%. With the increasing distance from the void area, the reduction rate for the vertical pressure of the soil layer gradually decreases. The main reason for this phenomenon is that the existence of the base void causes the soil layer to move to the void area, which then makes the soil layer discharge the load, and the density of the soil layer is reduced. As the distance from the hole increases, this effect gradually decreases, so the vertical pressure of measuring points C6–C8 is almost unchanged.

In actual heavy-haul railway operations, base softening will cause the deformation of the soil layer under the tunnel invert, and the density and bearing capacity will decrease. If the basement damage is not treated in time, the combined action of the train load and groundwater will accelerate the softening and hollowing speed of the basement soil layer and further reduce the bearing capacity of the basement.

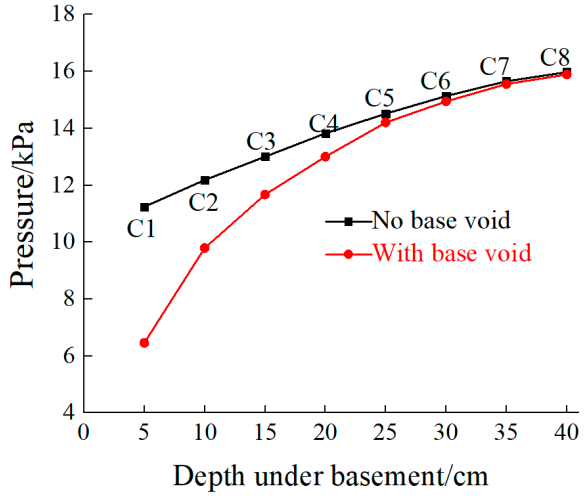


Figure 20. Peak vertical pressure of the soil layer below the tunnel invert.

6. Discussion

Based on the statistical results of base damage detection of a heavy-haul railway tunnel, a scale test of tunnel has been established. The dynamic response characteristics of a heavy-haul railway tunnel structure and the surrounding soil under the conditions of healthy base and base void have been studied. The base voids change the tunnel dynamic response, deteriorate the stress state of the structure, and shorten the fatigue damage life of the tunnel. In particular, the base voids have a great impact on the structure within the void range. The research results have certain reference value for similar tunnel tests. However, only one form of base void has been discussed in this test; in future studies, it can simulate the heavy-haul trains with different axial weights or speeds by changing values or frequencies of the output load of the vibrator, or it can change the width or length of the base voids to further enrich the research results. To facilitate the installation of the sensors, the scale model did not consider the inverted arch filling layer and the rail plate. Thus, there is a difference between the test results by using the present scale model and the actual situation. In the future, it is planned to assess one or one set of reduction coefficients through the field test data, so that the test results of this paper can been applied in real life.

7. Conclusions

The following conclusions can be drawn from this study:

(1) The experiment shows that the tunnel base void significantly increases the acceleration of the tunnel invert, while the effect for the test points outside the base void area is significantly reduced. The decay rate of the axial acceleration of the tunnel invert is slightly greater than that of the tunnel annular acceleration. This is mainly because the circumferential construction joints reduce the conduction efficiency of the vibration wave.

(2) With the action of the vibration force, the internal surface of a tunnel invert is mainly compressive stress, the external surface is tensile stress, and the stress value is constantly changing. When the tunnel has a base void, the peak surface stress of the invert increases by 21.3%, and the amplitude of the stress change increases by 0.56%.

(3) The acceleration of the soil decays with the increasing distance from the vibration source. The base void weakens the conduction efficiency of the nearby soil layer vibration and reduces the acceleration response of the soil layer. The acceleration response of the soil above the vault is small, and the attenuation speed is also significantly reduced.

(4) The soil near the base void deforms, and the density and bearing capacity decreases. If the tunnel continues to work with "damage" at this time, the range of the base softening or void will increase rapidly, seriously threatening the safe operation of the train.

Author Contributions: Conceptualization, L.G. and J.L.; testing, L.G. and T.C.; validation, L.G. and D.W.; investigation, L.G.; data curation, L.G., D.W. and G.W.; writing—original draft preparation, L.G.; writing—review and editing, D.W., J.L. and T.C.; visualization, T.C., D.W. and G.W.; supervision, J.L.; project administration, L.G and J.L. All authors have read and agreed to the published version of the manuscript.

Funding: This research received no external funding.

Institutional Review Board Statement: Not applicable.

Informed Consent Statement: Not applicable.

Data Availability Statement: Data is contained within the article.

Acknowledgments: The authors would like to thank all the anonymous reviewers for their meticulous comments and helpful suggestions.

Conflicts of Interest: The authors declare no conflict of interest.

References

1. Xia, S.C.; Yang, H.; Zhang, J.C. Research on the development model of heavy haul railway in China. *Railw. Transp. Econ.* **2011**, *33*, 9–13.
2. Geng, Z.X.; Li, X.F.; Zhang, B. Simulation study of heavy haul train operation on Datong-Qinhuangdao railway. *China Railw. Sci.* **2008**, *29*, 88–93.
3. Lv, W.Q.; Luo, Q.; Liu, G. Structural analysis and design method for subgrade bed of heavy haul railway. *J. China Railw. Soc.* **2016**, *38*, 74–80.
4. Zou, W.H.; Zhang, M.; Liu, Y.Q. Stress distribution and dynamic response of basement structure of heavy-haul railway tunnel under 30t axle load. *China Railw. Sci.* **2016**, *37*, 50–57.
5. Xue, J.L. Effect of tunnel bottom density on the stress of tunnel bottom structure and analysis of tunnel bottom reinforcement effect under 30t axle weight. *China Railw. Sci.* **2015**, *36*, 90–97.
6. Yin, C.F.; Fu, B.X.; Ma, W.B. Dynamic stress response of tunnel structures under heavy-haul trains. *China Railw. Sci.* **2013**, *34*, 47–52.
7. Ding, Z.D.; Peng, L.M.; Huang, J. Running safety in railway tunnel with base voids. *J. China Railw. Soc.* **2012**, *34*, 104–110.
8. Deng, B.; Qiao, C.; Yu, D.; Chen, S. Dynamic response analysis of heavy haul railway tunnel bedding structure. *Railw. Arch.* **2019**, *59*, 75–79.
9. Xu, X.L. Effect of tunnel bottom voiding on the stress of basement structure under the action of 30t axle heavy-haul train. *Railw. Eng.* **2014**, *4*, 44–49.
10. Liu, N.; Peng, L.M.; Shi, C.H. Effect of substrate conditions on dynamic response of heavy-haul railway tunnel structure and service life analysis. *Mod. Tunn. Technol.* **2016**, *53*, 114–122.
11. Xu, L.H.; Ma, M. Analytical solution of ground-borne vibration due to spatially periodic harmonic moving load on a tunnel embedded in layered soil. *J. Zhejiang Univ.-SCIENCE A.* **2023**, *In press*. [CrossRef]
12. Li, X.M.; Chen, Y.K. Building coupling loss measurement and prediction due to train-induced vertical vibrations. *Soil Dyn. Earthq. Eng.* **2023**, *164*, 107644. [CrossRef]
13. Zou, C.; Moore, J.A.; Sanayei, M.; Tao, Z.; Wang, Y. Impedance Model of Train-Induced Vibration Transmission Across a Transfer Structure into an Over Track Building in a Metro Depot. In *Journal of Structural Engineering*; ASCE: Reston, VA, USA, 2022; Volume 148.
14. Yang, W.; Hussein, M.F.M.; Marshall, A.M. Centrifuge and numerical modeling of ground-borne vibration from an underground tunnel. *Soil Dyn. Earthq. Eng.* **2013**, *51*, 23–24. [CrossRef]
15. Yang, W.B.; Chen, Z.Q.; Xu, Z.Y. Dynamic response of shield tunnels and surrounding soil due to train induced vibration. *Rock Soil Mech.* **2018**, *39*, 1–9.
16. Yuan, W.Z. *Similarity Theory and Static Model Test*; Southwest Jiaotong University: Chengdu, China, 1998.
17. Pak, R.Y.S.; Guzina, B.B. Dynamic characterization of vertically loaded foundations on granular soils. *J. Geotech. Eng.* **1990**, *121*, 274–286. [CrossRef]
18. Liang, B.; Luo, H.; Sun, C.X. Simulated study on vibration load of high speed railway. *J. China Railw. Soc.* **2006**, *28*, 89–94.
19. National Ministry of Railways of the Peoples Republic of China. *TB10003-2016 Code for Design on Tunnel of Railway*; China Railway Publishing House: Beijing, China, 2016.

Disclaimer/Publisher's Note: The statements, opinions and data contained in all publications are solely those of the individual author(s) and contributor(s) and not of MDPI and/or the editor(s). MDPI and/or the editor(s) disclaim responsibility for any injury to people or property resulting from any ideas, methods, instructions or products referred to in the content.